

# COLLECTIVE EXCITATION DYNAMICS IN MOLECULAR AGGREGATES: EXCITON RELAXATION, SELF-TRAPPING AND POLARON FORMATION.

M. Dahlbom, W. Beenken, V. Sundström, T. Pullerits

Department of Chemical Physics, Lund University, Box 124, S-221 00 Lund, Sweden

## 1 Introduction

The excited state properties and dynamics in various types of condensed systems are of great interest to the community of chemical physics. In particular, a diverse range of molecular systems where collective excited states occur has in recent time been under intense study due to their cooperative electronic behavior. Systems, such as conjugated polymers, fluorescent proteins and biological light-harvesting systems have attracted a great interest since ultra-short laser pulses became available and a large number of studies have been performed both theoretically and experimentally, see review<sup>1</sup> and references therein.

In these types of systems, the inter-molecular interactions can lead to delocalization of excited states, denoted exciton states (excitons). Molecular excitons were introduced by Frenkel<sup>2</sup> early in the last century and further studied by Davydov<sup>3</sup>. The properties and ultra-fast dynamics of cooperative excited state behavior in molecular aggregates have been studied extensively over the last decade. For example, a number of studies have utilized different techniques in order to characterize the exciton delocalization in bacterial photosynthetic antennas<sup>4,5</sup>. It has been suggested that an optical excitation in the tightly coupled peripheral antenna of purple bacteria spans a considerable size of the aggregate and relaxes within a few hundreds of femtoseconds to an equilibrium size of just a few chromophores<sup>5</sup>. Delocalized excitations can also be trapped at lattice sites due to the displacement of the excited state potential and the localization of the wave function as a result of the excitation-phonon coupling. Peierls<sup>6</sup> and Frenkel<sup>7</sup> introduced the possibility of exciton self-trapping as early as in the 1930's. Excitons that interact strongly with the nuclear degrees of freedom are denoted polarons. Due to this coupling they distort their surrounding to a considerable degree. Polaron formation has, for example, been suggested to occur in photosynthetic antenna aggregates at low temperatures<sup>8</sup>. Polaron with their sensitivity to nuclear motions can also be seen as possible non-destructive spectroscopic probes of protein and/or membrane dynamics.

The aim of this paper is to study the collective excitations coupled to the molecular vibrations in the real-space representation. We present a model that treats the molecular

vibrations classically via the Langevin equation whereas the electronic system is treated quantum mechanically<sup>9</sup>. The excitation dynamics can henceforth be studied as a function of the molecular vibrations. It will be shown that in the presented model, following an optical excitation, the excitons are trapped at low energy sites (self-trapping) due to the population enhancement of the displacement factor introduced via a mean field correction. The degree of excitation migration and self-trapping depends on temperature, exciton-phonon couplings (Huang-Rhys factors) and static distribution of site energies<sup>10,11</sup>. Special interest is directed towards the real-space motion of the excitation on the femtosecond time-scale and polaron formation. In order to distinguish between the two processes, we studied the wave function mobility and localization as a function of the vibrational frequency, displacement, temperature and intermolecular interaction strength. Besides the general considerations of real-space excitation dynamics in molecular aggregates on the femtosecond time-scale there is also the question of large scale energy funnelling in photosynthetic light-harvesting pigment-protein systems. In order to make the transfer between the B850 aggregate and the LH1 antenna complex more efficient in purple bacteria, the excitation in the B850 ring should be localized at the junction where the distance to the LH1 is the closest. Polivka et. al.<sup>8</sup> has attributed the appearance of a red-shifted feature in the transient absorption spectra at cryogenic temperatures to polaron formation. They propose that the polaron may be formed in inter-ring connection points. We will not address this problem specifically in the current work, but rather address the global aspects of the polaron formation as a viable process in photosynthetic light-harvesting systems.

## 2 THEORY

According to the Born-Oppenheimer approximation we separate the electronic degrees of freedom from the nuclear motion. The electronic system will be treated quantum mechanically in the molecular exciton picture<sup>2,3</sup>, while for the nuclear motion a classical approach will be used. Furthermore, the nuclear system will be separated into explicit and bath modes. The explicit modes are assumed to be coupled the electronic system via the adiabatic potential energy surface. To take into account the nonadiabatic coupling of the electronic system to the explicit modes, we use Tully's surface-hopping method<sup>9</sup>. The other modes will be described by use a Caldeira-Leggett<sup>10</sup> type of bath resulting in statistically fluctuating external forces driving and damping the explicit modes.

### 2.1 Frenkel Excitons

According to the Born-Oppenheimer approximation<sup>12</sup> the molecular electronic Hamiltonian is given by

$$H_{el} = \sum_i \frac{\hbar^2}{2m_i} \nabla_i^2 - \sum_{i,n} \frac{e^2 Z_n}{|r_i - R_n|} + \sum_{i,j \neq i} \frac{e^2}{|r_i - r'_j|}, \quad (1)$$

where  $r_i$  and  $r'_j$  assign electronic coordinates and  $R_n$  the nuclear ones with index  $n$  denotes the nuclear coordinate.  $\hbar^2 \nabla_i^2$  represents the electron momentum and  $m_i$  the corresponding mass. The nuclear charges are denoted as  $Z_n$ . In what follows, it has been assumed that the multi-electron problem is solved for the single molecule to obtain the single molecule energies as  $h_j$ , and the excitation creation and annihilation operators  $B_j^\dagger$  and  $B_j$ , respectively, where  $j$  denotes the molecular site<sup>13</sup>. The creation and annihilation operators are given by

$$B_j^\dagger = \sum_{a>b} b_{jab} a_a^\dagger a_b, \quad (2)$$

where  $a_a^\dagger$  and  $a_a$  are the creation and annihilation operators for electrons in the molecular orbitals  $|a\rangle$  and  $|b\rangle$ , and  $b_{jab}$  are the corresponding expansion coefficients. Due to the adiabatic approach the single molecule energies  $h_j$  as well as the operators  $B_j^\dagger$  and  $B_j$  depend parametrically on the nuclear coordinates  $R_n$ . The electronic Hamiltonian can be written in the excitonic representation as

$$H_{el}(R_n) = \sum_j h_j(R_n) B_j^\dagger B_j + \sum_{j,i \neq j} J_{ji}(R_n) B_j^\dagger B_i, \quad (3)$$

where  $J_{ji}$  describes the excitation transfer matrix elements between different molecules (depending on nuclear coordinates  $R_n$  as well). For sake of simplicity we will restrict our consideration to molecules that are well described as two level systems. Introducing the molecular ground and excited states as  $|\phi_j^{(g)}\rangle$  and  $|\phi_j^{(e)}\rangle$ , respectively, we can expand the exciton eigenstates as

$$|\alpha\rangle = \sum_j \left( c_{\alpha j}(R_n) |\phi_j^{(e)}\rangle \prod_{i \neq j} |\phi_i^{(g)}\rangle \right). \quad (4)$$

These states can be obtained by solving the eigenvalue equation

$$\langle \alpha | H_{el}(R_n) | \beta \rangle = U_\alpha(R_n) \delta_{\alpha\beta} \quad (5)$$

The eigenstates  $|\alpha\rangle$ , as well as the expansion coefficients  $c_{\alpha j}(R_n) = \langle \alpha | \phi_j^{(e)} \rangle$ , are dependent on the nuclear coordinates  $R_n$ . The eigenvalues  $U_\alpha(R_n)$  yield the adiabatic potential energy surfaces for the nuclear motions as

$$U_\alpha(R_n) = \sum_j \left( h_j^{(g)}(R_n) (1 - c_{\alpha j}^2(R_n)) + h_j^{(e)}(R_n) c_{\alpha j}^2(R_n) + \sum_{i \neq j} J_{ij}(R_n) c_{\alpha i}(R_n) c_{\alpha j}(R_n) \right), \quad (6)$$

depending on the nuclear coordinates  $R_n$  via  $h_j^{(g)}(R_n)$ ,  $h_j^{(e)}(R_n)$ ,  $J_{ij}(R_n)$  and  $c_{\alpha_j}(R_n)$ .

After transformation of the nuclear coordinates  $R_n$  to molecular normal coordinates  $q_{\mu,j}$  as performed in the next section, for an aggregate consisting of two-level system molecules one can write down the diagonal matrix elements of the general electronic Hamiltonian in the site representation as

$$H_{jj}^{(el)}(t) = E_j - \sum_{\mu}^M \omega_{\mu,j} d_{\mu,j} q_{\mu,j} \cdot \quad (7)$$

Here  $\mu$  denotes the  $M$  different explicit modes with frequency  $\omega_{\mu,j}$  belonging to the  $j$ 'th molecule.  $d_{\mu,j}$  is the displacement between the minima of the excited and ground state potential energy surfaces, and  $E_j$  the energy gap between excited and ground state for  $q_{\mu,j} = 0$ , means minimum of the ground state potential surface. This Hamiltonian is taken in the Frank-Condon approximation and both, the ground and excited state potential energy

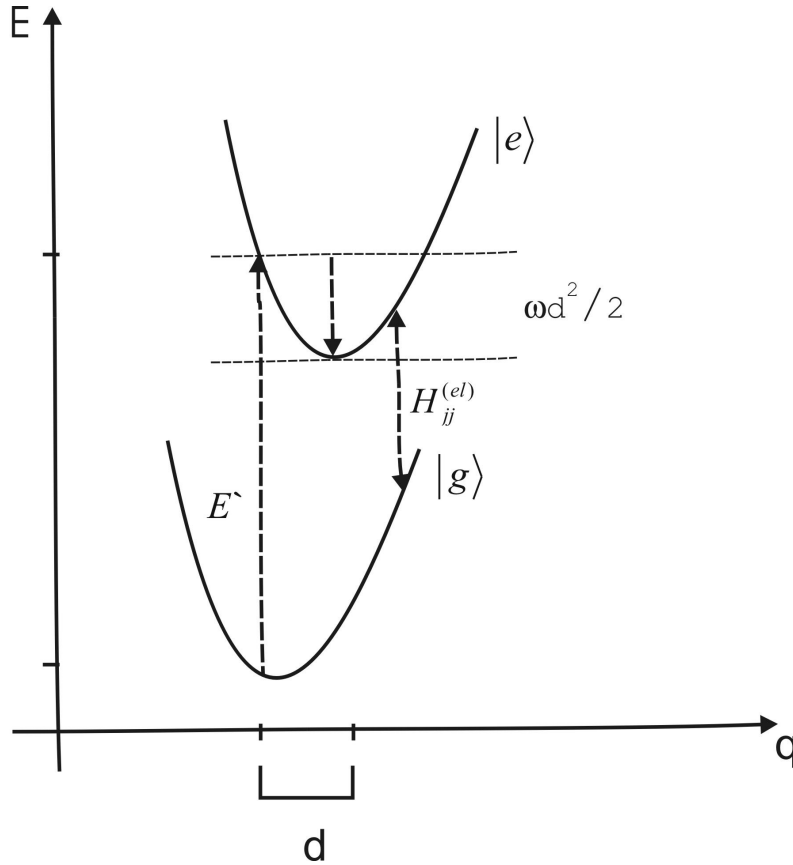


**Figure 1.** The two level schemes used for the individual molecules where the energy of the direct Frank-Condon transition from the ground state is  $E'$  and the energy gap is  $H_{jj}^{(el)}$ .

surfaces are taken to have same slope means frequencies  $\omega_{\mu,j}$ .

In the present work, we restrict ourselves to one explicit mode per molecular site with a unique frequency  $\omega$  and displacement  $d$ . If also the energy gap is site independent, Eq. (7) simplifies to

$$H_{jj}^{(el)}(t) = E + \hbar\omega d q_j. \quad (8)$$

## 2.2 Explicit Modes

In the gas-phase the molecular nuclear system can be described by three kinds of motion: translation, rotation and vibration. In the condensed phase the surrounding matrix hinders the first two. Nevertheless, it is useful to distinguish between inter-molecular motion, which means that the whole molecule changes its position relative to the neighbors; and intra-molecular motion, which means that the nuclei of a single molecule change their position and orientation in respect to each other. Inter-molecular motion will mainly affect the interaction matrix  $J_{ij}(R_n)$ , while intra-molecular motion has also an effect on the site energies  $h_j^{(g)}(R_n)$  and  $h_j^{(e)}(R_n)$ . In what follows, we will neglect the inter-molecular motion and focus on the intra-molecular motion. Expanding the ground state potential energy surface  $h_j^{(g)}(R_n)$  of site  $j$  around its minimum at  $R_n^{(j)}$  one can write

$$h_j^{(g)}(R_n) = h_j^{(g)}(R_n^{(j)}) + \sum_{n,m} \frac{\partial^2 h_j^{(g)}}{\partial R_n \partial R_m} (R_n - R_n^{(j)})(R_m - R_m^{(j)}) + \dots. \quad (9)$$

By transformation to principal axis we obtain a multidimensional harmonic oscillator potential in the normal mode representation, given by

$$h_j^{(g)}(q_{j\xi}) = h_j^{(g)}(0) + \sum_{\xi} \hbar\omega_{j\xi} q_{j\xi}^2 \quad (10)$$

using dimensionless coordinates  $q_{j\xi}$ . The excited state potential  $h_j^{(e)}(R_n)$  of site  $j$  can be expanded using the same coordinates as

$$h_j^{(e)}(q_{j\xi}) = h_j^{(e)}(0) + \frac{1}{2} \sum_{\xi,\xi'} \hbar\omega_{j\xi} W_{\xi\xi'} (q_{j\xi} - d_{j\xi})(q_{j\xi'} - d_{j\xi'}), \quad (11)$$

where  $W_{\xi\xi'}$  take into account a different curvature and  $d_{j\xi}$  a different minimum of the potential for the excited state. For sake of simplicity, the curvature of excited as well as ground state potential surface shall be unique too, i.e.  $W_{\xi\xi'} = \delta_{\xi\xi'}$ . Now one can deduce from Eqs.(6), (10) and (11) the excitonic potential surface as

$$U_\alpha(\dots q_j \dots) = E + \frac{1}{2} \sum_j \hbar \omega_j q_j^2 - \sum_j \hbar \omega_j q_j d_j c_{\alpha j}^2 + \sum_{i,j} J_{ij} c_{\alpha i} c_{\alpha j}, \quad (12)$$

One has to note that the  $c_{\alpha j}$  still depends parametrically on  $q_j$ . The potential surface given in Eq. (12) will be used to determine the intrinsic forces for the nuclear motion with respect to the site mode  $j$  as

$$F_{\alpha j}(\dots q_j \dots) = -\frac{1}{\hbar} \left\langle \frac{\partial U_\alpha(\dots q_j \dots)}{\partial q_j} \right\rangle = -\omega_j (q_j - d_j c_{\alpha j}^2) \quad (13)$$

Thus Eq. (13) leads us to Hook's force law. This is the core of our theoretical model.

### 2.3 Bath Modes

The complete Hamiltonian for the nuclear motion on the potential surface  $U_\alpha(\dots q_j \dots)$  is given by

$$\langle \alpha | H_{nuc} | \alpha \rangle = \frac{1}{2} \sum_j \hbar \omega_j p_j^2 + U_\alpha(\dots q_j \dots) + \frac{1}{2} \sum_\xi \hbar \omega_\xi (p_\xi^2 + q_\xi^2) + \sum_{j,\xi} K_{j\xi} q_j q_\xi. \quad (14)$$

Here the index  $\xi$  assigns the bath modes, while the index  $j$  assigns the explicit site modes as above. Following Caldeira-Leggett<sup>10</sup>, the bath modes are assumed to be harmonic oscillators and the coupling between bath and explicit modes to be bilinear in the coordinates  $q_j$  and  $q_\xi$  with coupling parameter  $K_{j\xi}$ . The dimensionless momentum  $p_{j,\xi}$  are related to the coordinates  $q_{j,\xi}$  by the canonical equations

$$\dot{q}_{j,\xi} = \frac{1}{\hbar} \left\langle \frac{\partial H_{nuc}}{\partial p_{j,\xi}} \right\rangle = \omega_{j,\xi} p_{j,\xi} \quad (15)$$

$$\dot{p}_{j,\xi} = -\frac{1}{\hbar} \left\langle \frac{\partial H_{nuc}}{\partial q_{j,\xi}} \right\rangle. \quad (16)$$

Resolving these canonical equations for the explicit mode and treating the bath modes statistically (see ref.10 for details), Eq. (16) results in the equation of dissipative nuclear motion

$$\dot{p}_j + \int_{-\infty}^t \gamma_j(t-t') p_j(t') dt' = F_{\alpha j}(\dots q_j \dots) + f_j(t), \quad (17)$$

where the intrinsic forces  $F_{\alpha_j}(\dots q_j \dots)$  are given by Eq. (13). The stochastical bath forces  $f_j(t)$  are connected to the dissipation, which is given by  $\gamma_j(\tau)$ , according to the dissipation-fluctuation theorem as

$$\langle f_j(t)f_j(t-\tau) \rangle = \gamma_j(\tau) \langle p_j^2 \rangle \quad (18)$$

For a thermalized bath the momentum variance  $\langle p_j^2 \rangle$  is given by

$$\langle p_j^2 \rangle = \frac{1}{\exp[\hbar\omega_j/k_B T] - 1} + \frac{1}{2} \quad (19)$$

If one neglects the memory of the bath, i.e. invokes the Markov approximation, Eq.(17) reduces to the Langevin equation<sup>12</sup>

$$\dot{p}_j(t) + \gamma_j p_j(t) = F_{\alpha_j}(\dots q_j \dots) + f_j(t), \quad (20)$$

where the integral  $\int_{-\infty}^t \gamma_j(t-t') p_j(t') dt'$  is substituted by the damping term  $\gamma_j p_j$ . The dissipation-fluctuation theorem time-averaged gives the variance of external forces  $f_j(t)$  as

$$\langle f_j^2 \rangle = \frac{2\gamma_j}{\tau^*} \left( \frac{1}{\exp[\hbar\omega_j/k_B T] - 1} + \frac{1}{2} \right), \quad (21)$$

where  $\tau^*$  is the correlation time of the fluctuations<sup>1</sup>.

### 3 NONADIABATICITY AND THE SURFACE HOPPING METHOD

In general, the time-dependent one-exciton wave function  $|\Psi(t)\rangle$  can be expanded in the adiabatic basis set  $|\alpha\rangle$  and propagated by

$$|\Psi(t)\rangle = \sum_{\alpha} C_{\alpha}(t) \exp\left[-\frac{i}{\hbar} \int_0^t U_{\alpha}(\tau) d\tau\right] |\alpha\rangle \quad (22)$$

---

<sup>1</sup> For the numerical calculations we will use random  $f_j(t_n)$  and set  $\tau^*$  equal to the time-step  $\Delta t = t_n - t_{n-1}$  of the propagation. This is justified because the value of  $f_j(t)$  will not change within the time interval  $[t_n, t_n + \Delta t]$ , which means that  $f_j(t)$  is fully correlated.

where  $C_\alpha(t)$  are time-dependent expansion coefficients. One has to note that the eigenfunctions  $|\alpha\rangle$  as well as the eigen-energies  $U_\alpha(t)$  are time-dependent due to the parametric dependency of the eigen-value problem Eq.(5) on the nuclear coordinates. These, now represented by normal coordinates  $q_j$  are propagating in time according Eq.(20). From Eqs.(4) and (15) one can deduce the identity

$$\hbar\omega\sum_j\langle\alpha|\frac{\partial}{\partial q_j}|\beta\rangle p_j = \sum_j c_{\alpha j} \frac{\partial c_{\beta j}}{\partial t} \quad (23)$$

for the nonadiabatic coupling between two excitonic eigenstates  $|\alpha\rangle$  and  $|\beta\rangle$ . The left side of the equality means that for a finite nuclear motion, i.e.  $p_j \neq 0$ , the adiabatic excitonic states are mixed by the nonadiabaticity of the electronic Hamiltonian beyond Born-Oppenheimer approximation<sup>12</sup>. On the right side the same coupling is represented by the time evolution of the coefficients  $c_{\alpha j}$ . The latter can be determined without explicit knowledge of their dependency on the coordinate normal coordinates  $q_j$  by diagonalisation of the excitonic Hamiltonian in the site representation, with diagonal elements  $H_{jj}$  as given in Eq.(8) and off-diagonal elements as  $H_{ij} = J_{ij}$ .

### 3.1 Surface Hopping Probability

Instead of a fully coherent propagation of the exciton, in this work we will apply the surface hopping method introduced by Tully<sup>9</sup>. Therefore, the time-dependent Schrödinger equation for the exciton wave function, given as

$$\frac{\partial}{\partial t}|\Psi\rangle = H(t)|\Psi\rangle, \quad (24)$$

is transformed into a system of differential equations for the coefficients  $C_\alpha(t) = \langle\alpha|\Psi\rangle$ , yielding as

$$\frac{dC_\alpha(t)}{dt} = -\sum_\beta k_{\alpha\beta}(t)C_\beta(t) \quad (25)$$

using transport coefficients given by

$$k_{\alpha\beta}(t) = \sum_j \left( c_{j\alpha} \frac{\partial c_{j\beta}}{\partial t} \right) \exp \left[ i \int_0^t \omega_{\alpha\beta}(\tau) d\tau \right], \quad (26)$$

where  $U_\alpha(\tau) - U_\beta(\tau) = \hbar\omega_{\alpha\beta}(\tau)$ . Since one can write down the probability to jump from a exciton eigen-state  $|\alpha\rangle$  to another  $|\beta\rangle$  within a time interval  $[t_0, t]$  as

$$P(\alpha \rightarrow \beta) = \int_{t_0}^t [k_{\beta\alpha}(\tau)\rho_{\beta\alpha}(\tau) - k_{\alpha\beta}(\tau)\rho_{\alpha\beta}(\tau)] d\tau \quad (27)$$

using the density matrix elements  $\rho_{\alpha\beta}(\tau) = C_\alpha^*(\tau)C_\beta(\tau)$ , the relation  $k_{\alpha\beta}^*(\tau) = -k_{\beta\alpha}(\tau)$ , Eq.(25) and where  $t_0$  is the time of the last hop. According to Eqs.(26) and (23) the transport coefficients  $k_{\alpha\beta}(\tau)$  are mainly determined by the nonadiabatic coupling. With other words,  $P(\alpha \rightarrow \beta)$  gives the probability for the nonadiabatic hopping between adiabatic potential surfaces. Between the jumps, the exciton propagation is performed coherently on the adiabatic potential surfaces due to the exponential term in Eq.(26).

### 3.2 The Surface Hopping Algorithm

In the surface hopping method, two sets of states are simultaneously followed, the reference and the auxiliary states. The latter are propagated using Schrödinger equation as discussed above and used for calculating the surface hopping probabilities. The populations on the auxiliary states are propagated coherently. The populations on the reference states are always 0 or 1; it will only change if the surface hopping occurs. In figure 2 below, the reference states are shown verses time and the thick black solid line corresponds to the populated state at that given point in time. The surface-hopping Algorithm can be defined by following steps:

(i) The system is initialized, as the electronic Hamiltonian at time zero is generated using a random distributed set of coordinates and momenta,  $\{q_i(0), p_i(0)\}$ , corresponding to the given system temperature. Solving the Schrödinger equation for this configuration one obtains the initial exciton energies and wave functions and the initial population can be created in a predefined manor. Note that at time zero the reference states and the auxiliary states are the same, which is not true for the following time steps.

(ii) The explicit mode oscillators are then propagated a time step  $\Delta t$  using the Langevin equation, Eq.(20), and the new electronic Hamiltonian is generated. The eigen-value problem is solved generating new states and energies. The populations on the reference states are always integer, but the populations on the auxiliary states are propagated according to Eq.(24).

(iii) Based on the auxiliary states the hopping probability for the reference configuration is calculated using Eq.(27). A random number  $\xi$  is pulled from a uniform distribution  $[0,1]$  and the population is moved from state  $|\alpha\rangle$  to  $|\beta\rangle$  if the criterion

$$\sum_{\beta' \neq \alpha, \beta'=0}^{\beta-1} P(\alpha \rightarrow \beta') < \xi < \sum_{\beta' \neq \alpha, \beta'=0}^{\beta} P(\alpha \rightarrow \beta') \quad (28)$$

is fulfilled. Otherwise the decision is taken not to jump. Then one continues with step (ii).

### 3.2 Localization and Motion of Excitons

As discussed in the Introduction, the states in a molecular aggregate with a sufficiently large intermolecular interaction will be more or less delocalized and one usually denotes them as exciton states. If, however, the excitons couples strongly to the (intra- or inter-) molecular vibrations, localization may occur, this means polaron formation. In our model the polaron formation results from a feedback between excitonic and nuclear Hamiltonian, as follows: Since the exciton states are delocalized to some degree by dipole-dipole interaction, each individual molecular site will contribute only a certain amount to the exciton wave-functions according to Eq.(4). However, the displacement  $d$  is weighted with these contributions to give the internal forces in Eq.(13). For occupation of the lowest excitonic state, these forces will drive the molecular site that contributes most to the exciton wave-function to a lower molecular site energy. Consequently, this site will give a still higher contribution to the lowest excitonic state than before. This results in a self-amplifying increase of the exciton localization. Likewise the mobility of the exciton decreases - eventually up to self-trapping - since it becomes harder for the excitation to slip out of the trap to a neighboring site. Nevertheless due to Eq. (20) at finite temperature the external forces from the thermal bath may statistically kick the system out of the self-trapping configuration. On the other hand, for small displacements localized polarons will not be formed. In this case only the center of the delocalized excitonic wave function may fluctuate thermally, due to the kicking bath forces.

To study the localization quantitatively we use the customary inverse participation ratio, defined as

$$L_{pr}^{-1}(t) = \frac{1}{Z} \sum_{j,\alpha} c_{\alpha j}^4 \rho_{\alpha\alpha}(t) \quad (29)$$

where the  $c_{j\alpha}(t)$  are the parametrically time dependent expansion coefficient of the exciton eigen-state  $|\alpha\rangle$ . The diagonal density matrix element  $\rho_{\alpha\alpha}(t)$  is just the population of this eigen-state and results from Eq.(25).  $Z$  represents the normalization factor<sup>5</sup>. In order to analyze the mobility of the exciton we begin by introducing the exciton (polaron) position operator  $\hat{Q} = \sum_j j B_j^\dagger B_j$ , following Mak et. al.<sup>14</sup>, to obtain

$$Q(t) = \sum_{\alpha,j} j c_{\alpha j}^2(t) \rho_{\alpha\alpha}(t). \quad (30)$$

This quantity gives information on which site is the center of gravity of a localized as well as a delocalized excitation. However, it can trace the motion of an exciton only for single

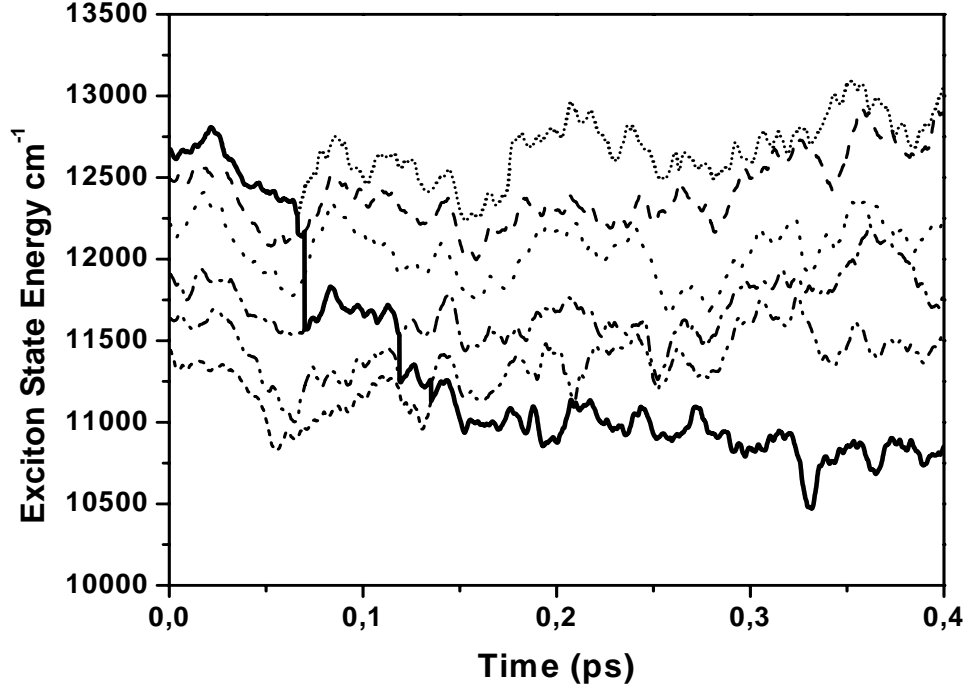


**Figure 2.** The energies for the electronic states overlaid with the current reference state (thick solid line). The Huang-Rhys factor is 1.125 and the temperature 0K.

Monte-Carlo trajectory. For sampling over a huge amount of trajectories on homogeneous aggregates it yields only a constant averaged value. In order to remedy this situation, we define the velocity of an exciton as

$$I(t) = \left| \frac{dQ(t)}{dt} \right| \quad (31)$$

which will be not canceled by the Monte-Carlo averaging. If the velocity has a high value, the exciton moves rapidly through the system, probably on a random walk. However, if the value of  $I(t)$  is small the interpretation is ambiguous: either the exciton is trapped, e.g. by “small” polaron formation, or it is delocalized in such a degree, that its motion does not result in a significant change of the site populations. The second kind of interpretation can be only excluded, if both,  $I(t)$  and  $L_{ipr}(t)$  are small, means the exciton is trapped and localized on mainly one site.

## 4 RESULTS AND DISCUSSION

The model system considered here is a linear aggregate of six identical two-level systems with the molecular optical transition at  $12400\text{ cm}^{-1}$  and a value of the nearest neighbor intermolecular interaction set to  $342\text{ cm}^{-1}$  for all sites. We restrict ourselves to a single explicit intra-molecular uncorrelated vibrational mode per molecular site with a

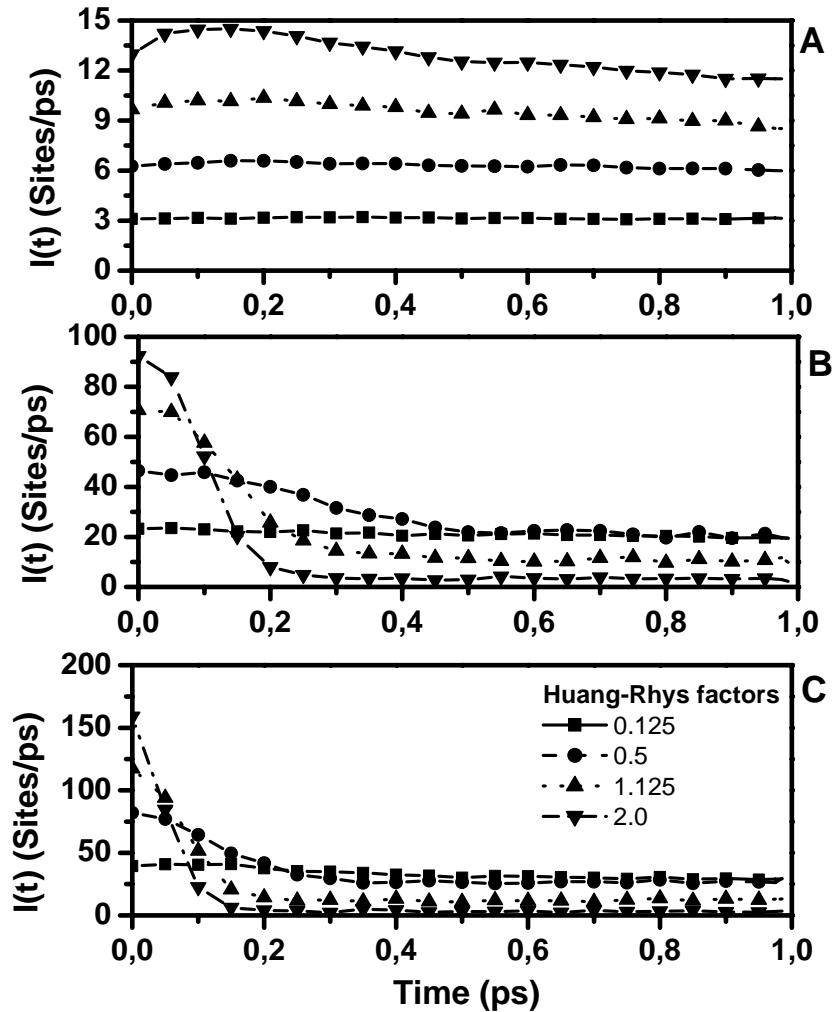


**Figure 3.** The exciton (polaron) velocity as a function of time, where panel A displays  $\omega_{\text{vib}}$  equal to  $250\text{ cm}^{-1}$ , B  $684\text{ cm}^{-1}$ , C  $900\text{ cm}^{-1}$ . The symbols are displayed in the legend of panel C.

unique vibrational frequency and displacement  $d$ .

The electronic level dynamics is displayed in figure 2. The excitonic states are displayed using different line styles; the thick solid line represents the currently populated reference level. In the displayed case the population has relaxed to the lowest exciton state in a few hundred femtoseconds. On the longer time scale the broadening of the energetic band gap can be seen.

For detailed analyzing of the polaron formation we start to figure out the influence of the displacement  $d$  (expressed as Huang-Rhys factors  $S = 0.5 d^2$ ) on the localization ( $L_{ipr}(t)$ ) and the exciton velocity ( $I(t)$ ) of the exciton. Figures 3 and 4, where the Huang-Rhys factor is varied between 0.125 and 2.0. shows the strong dependence of both quantities on the mode frequency and displacement (Huang-Rhys factors). The influence of the displacement on  $I(t)$  and  $L_{ipr}$  is easy to understand since it controls the molecular

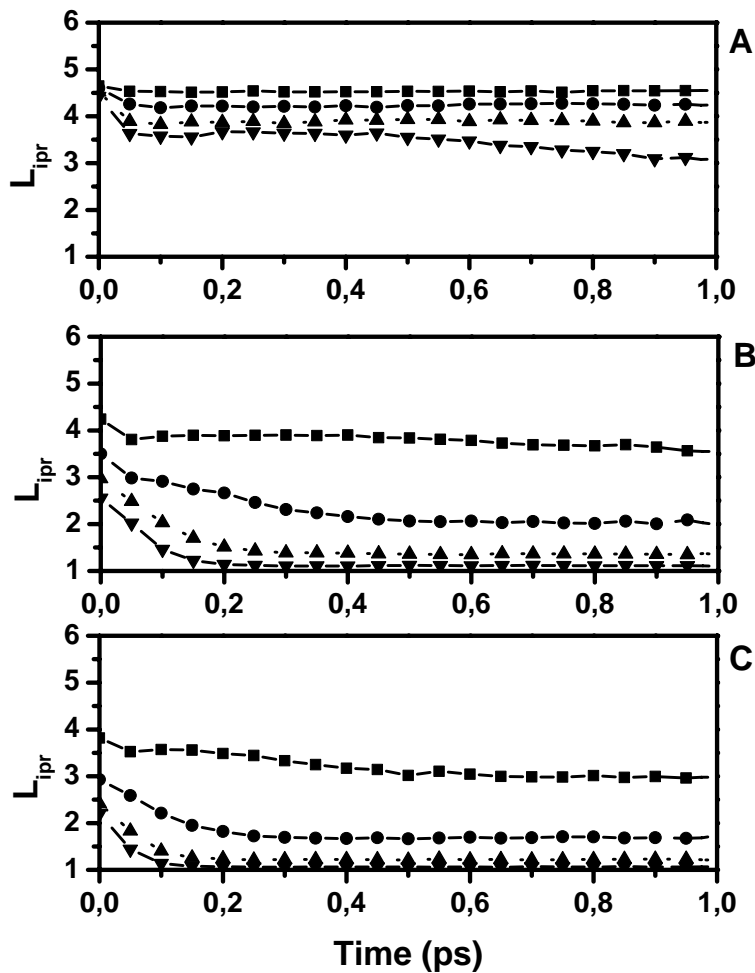


**Figure 4.** The inverse participation ratio displayed as a function of time. The symbols and parameters are the same as in figure 3.

energy gap according to Eq.(8). Due to the feedback channel in the Langevin equation, the exciton-phonon coupling increasingly influences the localization.

We know from the dimer that the inter-level transfer rates are maximized if the vibrational frequency is tuned to twice the inter-molecular interaction energy. In this case the vibrational frequency matches exactly the energy gap between the levels and a resonance occurs. We tuned the inter-molecular vibrational frequencies from  $250 \text{ cm}^{-1}$  as shown in Panel A,  $642 \text{ cm}^{-1}$  Panel B up to  $900 \text{ cm}^{-1}$  as in Panel C. There is a fast initial rise followed by a monotonic decrease in all kinetics in figure 3, panels A through C. Even though the time-scales change, the dynamics behaves similarly in all three cases, i.e. the velocity decrease as the vibrational frequency increase.

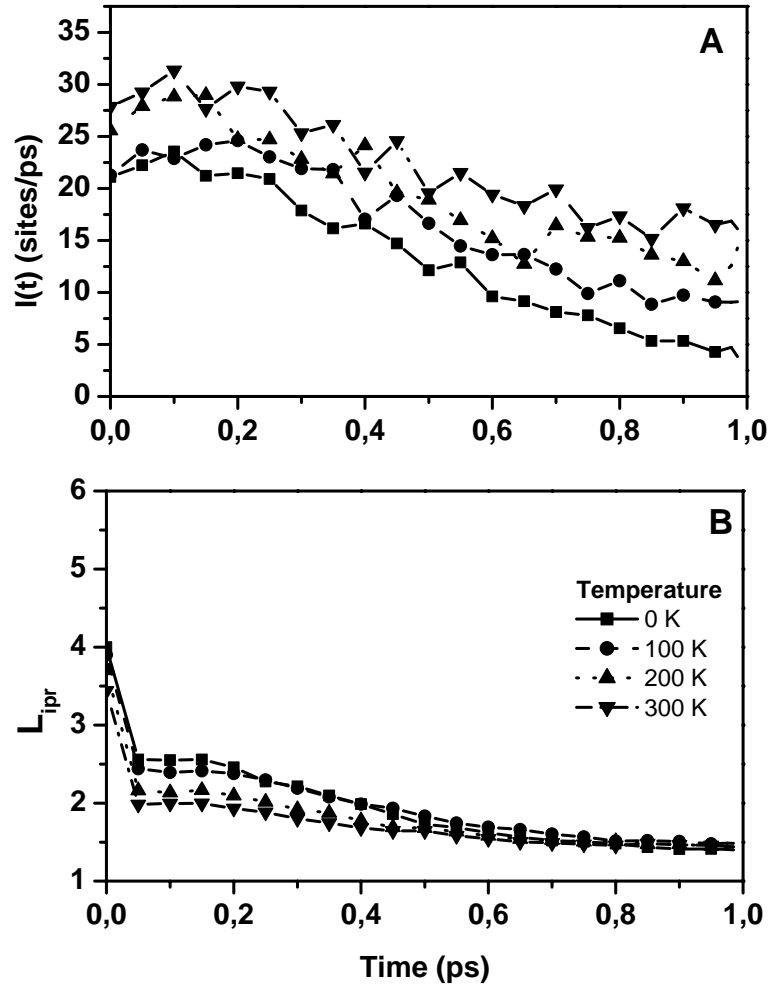


**Figure 5.** The time-dependence exciton velocity and inverse participation ratio displayed for four different temperatures. Intermolecular coupling  $V= 100 \text{ cm}^{-1}$ ,  $\omega=200\text{cm}^{-1}$  and the Huang-Rhys factor is 1.125.

In figure 4, there is a fast initial decrease of  $L_{ipr}$  followed by a slower phase present in all the three cases. From the frequency dependence, we conclude that the polaron formation occurs faster at higher vibrational frequencies. Further, it is clear that even for very low temperatures, where the vibrations are almost negligible, polaron formation depends on the ratio of the inter-molecular interaction and the Huang-Rhys factor multiplied with the vibrational frequency. Stated differently, polaron formation does not occur until the

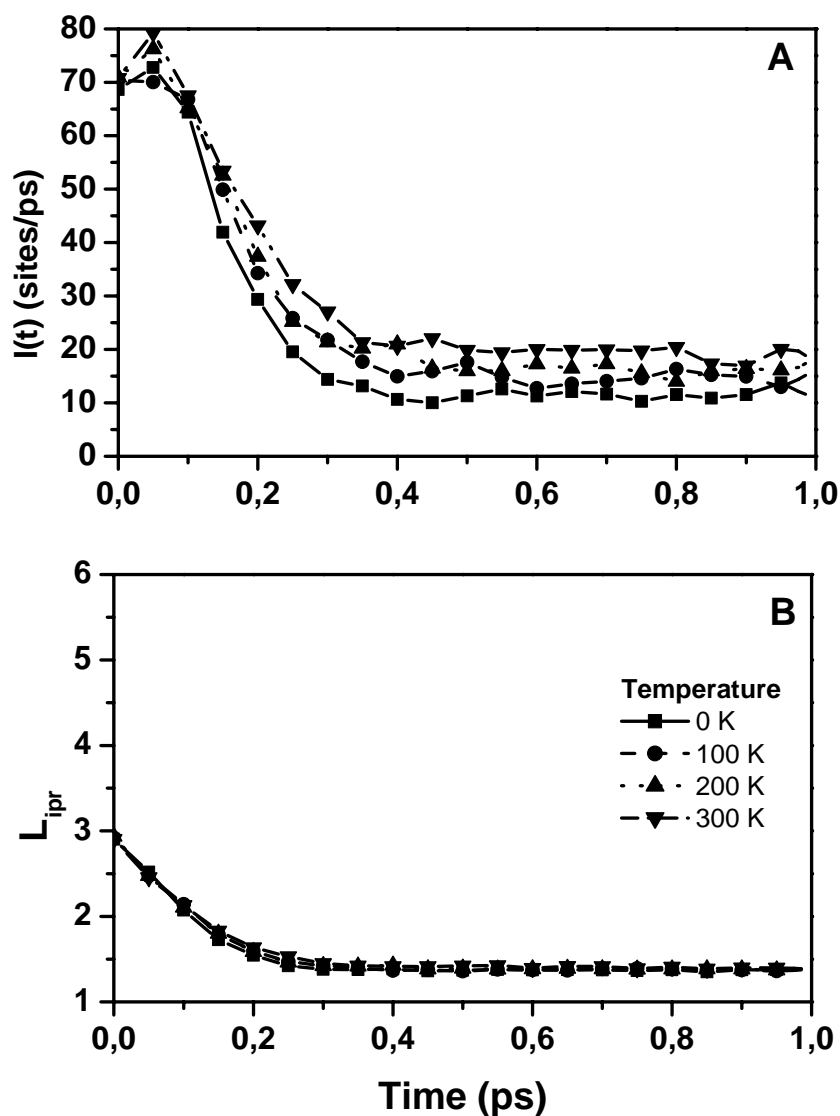


**Figure 6.** The exciton velocity and inverse participation ratio, with a intermolecular coupling  $V= 342 \text{ cm}^{-1}$ ,  $\omega=684\text{cm}^{-1}$  in the hexamer model system, as a function of temperature. The Huang-Rhys factor is 1.125.

coupling between the nuclear and electronic degrees of freedom become sufficiently strong to overcome the delocalization of the intermolecular dipolar coupling.

Next we turn our attention to the temperature dependence for the inverse participation ratio ( $L_{ipr}$ ) and the exciton velocity ( $I(t)$ ). The important parameter for the temperature dependence is the ratio of the vibrational quantum and the thermal energy  $\omega_{vib}/kT$ . We performed two sets of simulations; the first with  $V=100\text{ cm}^{-1}$  and  $\omega_{vib}=200\text{ cm}^{-1}$ . The temperature was varied from 0 to 300 K. The second set was done exactly in the same way, but for  $V=342\text{ cm}^{-1}$  and  $\omega_{vib}=684\text{ cm}^{-1}$ . Figure 5 displays the first case with panels of both, the exciton velocity (see panel A) and the inverse participation ratio (panel B) and in Figure 6 corresponding data is displayed for the second scenario. In Figure 5, the ratio between vibrational and thermal energy is close to unity, and temperature dependence is clearly visible. The velocity ( $I(t)$ ) at time zero is a factor of 1.5 larger for 300K than for 0K, but after 1ps the velocity at 300K is nearly twice as large as at 0K. In panel B, the inverse participation ratio ( $L_{ipr}$ ) is displayed as a function of time and temperature. Here the temperature dependence is slightly, but still clearly visible below 400fs, indicating the importance of the ratio  $k_B T/\hbar\omega$  mentioned above. In Figure 6, the ratio between the intermolecular vibrational frequency and thermal energy is much larger than unity. There is weak temperature dependence visible in panel A. The final velocity for the different temperatures lies between 10 and 20 sites/ps.

For all temperatures the inverse participation ratio is between 1 and 2 molecules. However, the time dependence of the velocity  $I(t)$  and the inverse participation ratio  $L_{ipr}$  is qualitatively similar for all temperatures. The apparent difference between the panels in figure 5 and 6 is deceiving. Due to the lower interaction energies and vibrational frequencies only the time scale is shifted. If one takes this into consideration the two panels show very similar time dependence.

Finally we want to turn the attention to the exciton band gap of the molecular aggregate. The polaron formation will involve a lowering of the energy of a specific site due to the feedback channel introduced in Eq.(13), hence causing the lowest exciton energy to decrease and widening the exciton band. The band gap is here defined by the energy difference between the lowest and highest exciton states and is displayed in the two panels in Figure 7. Panel A shows the averaged exciton energies and panel B the time-dependent band gap. In figure 7 two effects can be seen when the exciton-phonon coupling is increased. The increase of the band gap due to the increase of the molecular site fluctuations, i.e. the increase of the slope in panel A and the initial rise in panel B. Secondly, the polaron formation due to the decrease of the lowest exciton state energy so that it energetically deviates from the rest of the equally spaced exciton energy levels. The first effect arises from the displacement dependent Hamiltonian in Eq.(8) which causes the energy fluctuations of the excitonic states to become larger with increasing Huang-Rhys factors. The decrease of the lowest exciton energy is a result of the polaron formation, i.e. the energetic trap is formed by the interaction of the localized exciton and the molecular vibrations on the occupied site. The second effect indicates that the polaron formation process has come into balance with the delocalizing effect of the inter-molecular

interactions. Further, it is clear that after a few hundred femtoseconds the band gap stays constant for all Huang-Rhys factors. This is caused by the exciton-vibrational coupling, since an increase of Huang-Rhys factor does not only lower the energy on the populated site but does also increase the amplitude of the molecular energy fluctuation.

To summarize, we have proposed a model, based on the surface-hopping method in the real-space (site) representation, capable of calculating the excitation dynamics in molecular aggregates where the molecular vibrations are incorporated on a real-time basis. We have

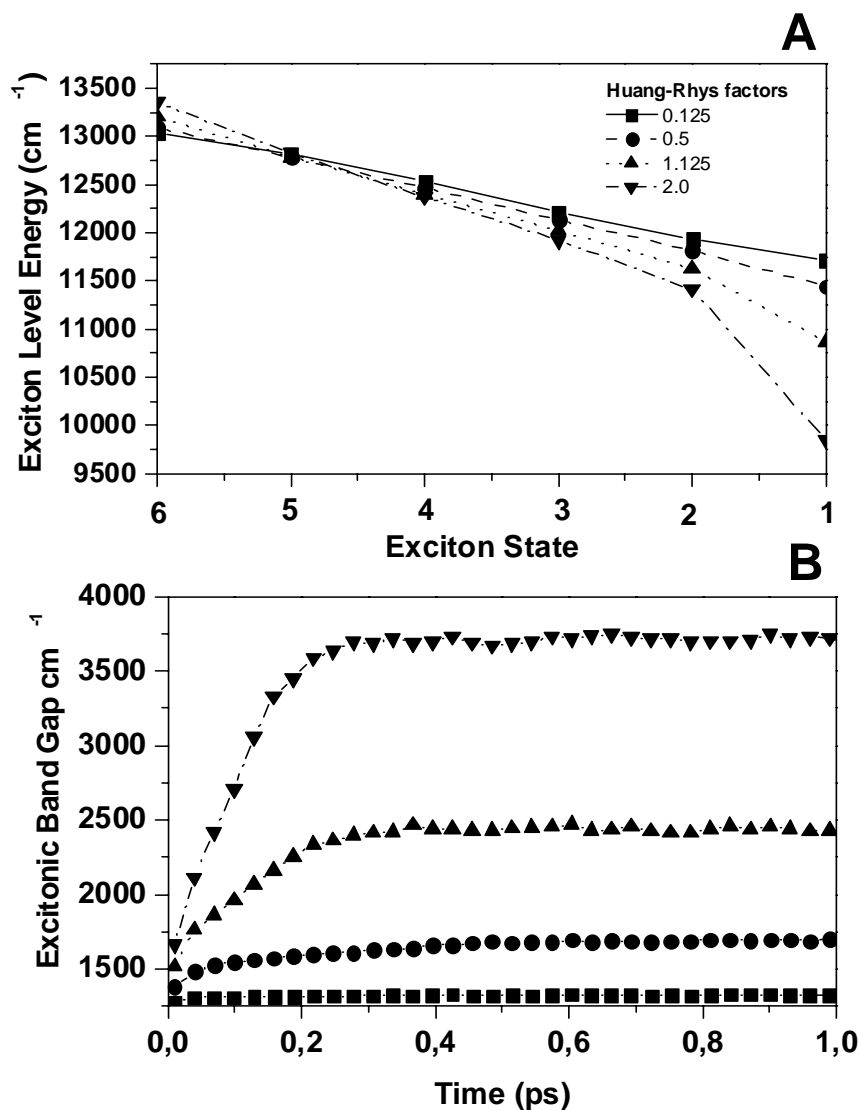


**Figure 7.** Panel A displays the exciton energies as a function of state number for four different realizations of the Huang-Rhys factor. Panel B shows the time dependent exciton band gap for the same Huang-Rhys factors as panel A. The parameters are the same as in figure 4.

shown that this model can capture such phenomena as polaron formation and self-trapping. The dependency on temperature, exciton-phonon coupling, phonon frequency and intermolecular interaction strength were investigated.

#### Reference:

1. V. Sundström; T. Pullerits; R. van Grondelle, *J. Chem. Phys. B* 1999, **103**, 2327.
2. J. I. Frenkel, *Phys. Rev.* 1931, **37**, 17.
3. A. S. Davydov, *Theory of Molecular Excitons*, Plenum Press: New York, 1971.
4. M. Dahlbom; T. Minami; V. Chernyak; T. Pullerits; V. Sundström; S. Mukamel, *J. Chem. Phys. B* 2000, **104**, 3976.
5. M. Dahlbom; T. Pullerits; S. Mukamel; V. Sundström, *J. Phys. Chem. B* 2001, **105**, 5515.
6. R. Peierls, *Ann. Phys.* 1932, **13**, 905.
7. J. I. Frenkel, *Phys. Z.* 1936, **9**, 158.
8. T. Polivka; T. Pullerits; J.L. Herek; V. Sundström, *J. Chem. Phys. B* 2000, **104**, 1088.
9. J. C. Tully, *J. Chem. Phys.* 1990, **93**, 1061.
10. U. Weiss, *Quantum Dissipative Systems*; World Scientific: Singapore, 1999.
11. S. Mukamel, *Principles of Nonlinear Optical Spectroscopy*; Oxford University Press: New York, 1995.
12. I.B. Bersuker; V.Z., Polinger *Vibronic Interactions in Molecules and Crystals*; Springer Verlag: Berlin, 1998.
13. F. C. Spano, *Phys. Rev. Lett.* 1991, **67**, 3424.
14. C. Mak; R. Egger, *Phys. Rev. E* 1994, **49**, 1997.